

# Fracture mechanics testing of fiber-reinforced polymer composites: The effects of the “human factor” on repeatability and reproducibility of test data

Andreas J. Brunner<sup>1</sup>

*Empa, Swiss Federal Laboratories for Materials Science and Technology, Laboratory for Mechanical Systems Engineering, Überlandstrasse 129, CH-8600 Dübendorf, Switzerland*

## ARTICLE INFO

### Keywords:

Fiber-reinforced polymer-matrix composites  
Fracture testing  
Intrinsic and extrinsic scatter  
Human operator effects  
Digital measurement technologies  
Additive manufacturing

## ABSTRACT

Fracture mechanics data from fiber-reinforced polymer-matrix (FRP) composites are required for damage-tolerant design. Quantifying scatter is essential for determining design limits. Scatter is affected by the “human factor”, i.e., process and test operator actions. Intrinsic scatter from manufacture, processing and environment shall be preserved; extrinsic scatter from specimen preparation, test set-up, measurement resolution, and analysis minimized. Automated processes yield fairly consistent scatter, but additive manufacturing of FRP composites has not reached the same maturity level yielding more defects or weak interfaces. The potential of digital technology for reducing scatter and quantifying single and multiple delamination propagation are also discussed.

## 1. Introduction

Fracture mechanics based damage-tolerant designs for FRP composite structures considering stable delamination propagation are expected to provide safe and light-weight solutions, e.g., for aircraft and space vehicles [1–4], but also for other transportation systems [5]. For this, fracture mechanics tests have to be developed and standardized, providing materials design data representative of cyclic fatigue fracture loads [4,6]. So far, fatigue fracture tests and the analysis for determining FRP design limits are still under development, see, e.g., [7–11]. The only available standard procedure for cyclic fatigue fracture of FRP deals with the onset of a Mode I delamination from an artificial starter crack [12].

However, the concept of FRP composite structural design allowing for a certain amount of slow, stable and predictable delamination propagation has recently been critically examined and several gaps in understanding and quantifying delamination propagation were pointed out [13]. One problem noted in this paper is the determination of the scatter in the experimental data for defining the design limits. In test method standards, a statement of accuracy is now usually required [14], but is not available in most earlier standards, e.g., [12,15]. Repeatability of a standard measurement method is typically determined by performing tests on one batch of material under nominally identical conditions in one lab by the same operator. One test procedure [16] even adds that the tests shall be performed the same day (obviously assuming that operator performance or environmental conditions may vary with time). Reproducibility is determined by performing tests on one or several, but nominally identical batches of material in several labs, but again with the same equipment and operator for each laboratory [17]. The use of such repeatability and reproducibility data is discussed in,

*E-mail address:* [andreas.brunner@empa.ch](mailto:andreas.brunner@empa.ch).

<sup>1</sup> Retired from Empa.

## Nomenclature

AE	Acoustic Emission
AI	Artificial Intelligence
AM	Additive Manufacturing
ASTM	American Society for Testing and Materials International
b	specimen width
CDD	Curvature Driven Delamination
CF	Carbon Fiber
CF-PEEK	Carbon Fiber Reinforced Poly-Ether-Ether Ketone
CF-PPS	Carbon Fiber Reinforced Poly-Phenylene-Sulfide
CFRP	Carbon Fiber-Reinforced Polymer (matrix)
CVr	coefficient of variation for repeatability (measured in %)
CVR	coefficient of variation for reproducibility (measured in %)
DCB	Double Cantilever Beam (specimen)
DIC	Digital Image Correlation
ENF	End-Notched Flexure (specimen)
ESIS	European Structural Integrity Society
FRP	Fiber-Reinforced Polymer (matrix)
$G_C$	Critical Energy Release Rate
$G_{IC}$	Critical Energy Release Rate for Mode I loading
GF-PMMA	Glass Fiber-Reinforced Poly-Methyl-Meth-Acrylate
GFRP	Glass Fiber-Reinforced Polymer (matrix)
ISO	International Organization for Standardization
ML	Machine Learning
Mode I	tensile opening load for fracture testing
Mode II	in-plane shear load for fracture testing
Mode III	out-of-plane twisting load for fracture testing
NDT	Non-Destructive Test
NL	non-linear point on load–displacement curve
TC4	Technical Committee 4
$\delta$	test machine displacement
2 h	(total) specimen thickness (thickness of half beam for symmetrical specimens is h)
3D	three-dimensional
5%	5% reduction in compliance point on load–displacement curve
5%/MAX	5% reduction in compliance or maximum load in load–displacement curve

e.g., [9,18].

There are a few examples of published repeatability and reproducibility data from fracture mechanics measurements on FRP, e.g., [16,19] the first one presenting selected data from [20]. Fig. 1 shows average  $G_{IC}$  data for AS4/PEEK composites taken from Tables 2 and 3 of [20] and the coefficients of variation for repeatability (in-laboratory scatter) and repeatability (inter-laboratory scatter), respectively. There is significant scatter between the different average round robin values, but a general trend with values increasing from NL to Vis to 5%, an effect that typically originates from increasing contributions of fiber-bridging with increasing delamination lengths. The scatter in both, repeatability and reproducibility likely is a combination from different sources. Both, in materials processing and testing, there are several aspects where operator decisions or actions may produce scatter and, hence, it is difficult to quantify these effects. First, the different test series in Fig. 1 were performed with different batches of AS4/PEEK, possibly prepared and processed by different people, and different batches had starter films made of different material types and/or with different thickness. Second, there is no information on the test operators performing tests at the different laboratories. Even for the same test operator, performance may vary with time (repeatability) and different operators may yield even larger test data scatter (reproducibility). The same test operator, for example, can acquire experience from one test series to the next, resulting in a reduction in scatter with the number of tests performed, but daily performance may still vary.

In Fig. 1 (right), for quasi-static Mode I tests the coefficients of repeatability (CVr) for in-laboratory scatter and for reproducibility (CVR), respectively do not yield a clear trend, in about half of them the reproducibility coefficient CVR is larger than CVr, and in the others roughly equal or clearly less. Minimum values of both, CVr and CVR are about 8% and maxima at about 14% for repeatability and, somewhat higher, around 18% for reproducibility. For quasi-static Mode II tests on composites, round robin values of the coefficient of repeatability (CVr) as low as 4–5% were observed for Mode II precracks, but were around 10% for testing from an insert film or a Mode I precrack [21]. The maximum CVr and CVR values reported for the Mode II tests both were higher than 20%. Larger scatter in Mode II than Mode I has been observed in other Mode II tests and indicates that Mode II loading may intrinsically yield larger scatter. This is possibly due to the more complex damage accumulation from delamination propagation in Mode II and the related problem of

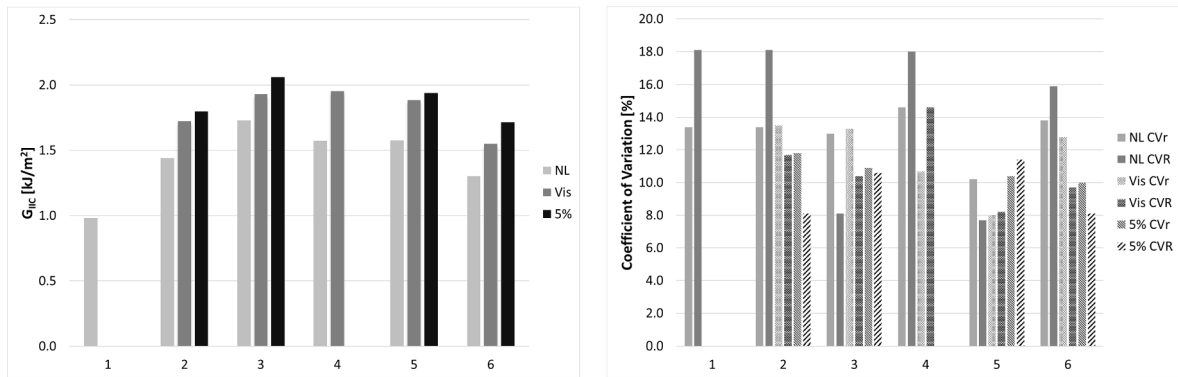


**Fig. 1.** (left) Average initiation values NL, Vis and 5% for AS4/PEEK of six test series (1–6) from four round robins with between three and sixteen laboratories testing three or four specimens each, (right) the respective coefficients of variation (standard deviation of mean  $G_{IC}$  value in %) for repeatability (CVr) and reproducibility (CVR); all data reported in [20].

identifying the delamination tip as discussed in section 3.6 below.

For defining design limits for FRP composite structures or components, it is essential to account for the variability due to the type of material, its processing and manufacture as well as machining and conditioning of the laminates or components, while other effects should be minimized. This leads to two classes of scatter, one caused by intrinsic and the other by extrinsic factors. As discussed in detail in [22] sources of extrinsic scatter comprise (cite) “... test set-up (e.g., compliance or play in the load-introduction, or load cell range with insufficient measurement resolution,), operator experience (e.g., learning curve for proper test set-up as well as visual observation during testing ...), but also machining variation in specimen width and cutting quality, or variation in laminate plate thickness (e.g., near the edges) affecting the individual specimens’ compliance ... which should be limited or excluded by proper test specification.”

It is likely that the “human factor”, i.e., aspects relating to process or test operator performance and experience, plays a significant role in determining intrinsic and extrinsic scatter [23]. The simplest example for extrinsic scatter is the visual observation of the delamination length by the operator during the tests. The “human factor” contribution to intrinsic scatter originates from manual materials processing and manufacturing steps, e.g., prepreg lay-up inducing variation in fiber orientation, mixing of resin and additives with variation in concentrations, or by control of resin infusion speed.

The present contribution hence looks at the “human factor” effects on intrinsic and extrinsic scatter in fracture tests of FRP composites and how scatter can possibly be reduced through state-of-the-art digital technology in processing, manufacture, measurements and data analysis. The challenges of dealing with multiple delaminations or defect sites are also briefly discussed, specifically in the context of FRP made with AM processes.

## 2. Materials and methods

The materials discussed and the methods used for the analysis are described in the references cited in the text. The presentation focusses on FRP composites, either CFRP or GFRP made by lamination processes or AM. The test methods are fracture mechanics based, both standardized by, e.g., ISO or ASTM, for details see the cited references.

## 3. Sources of scatter in fracture data of FRP: Selected issues and discussion

### 3.1. Intrinsic versus extrinsic scatter sources

Intrinsic scatter basically represents the variation in FRP laminate morphology with the specific polymer matrix, fiber lay-up, but also the microscopic and *meso*-scale defect types and distribution(s) as well as internal stresses resulting from laminate processing [22]. Beside material processing, test specimen preparation and conditioning, which, at least in research laboratories, mainly are still performed manually, also contribute to scatter. A potential source of intrinsic scatter beyond test specimens are changes of quality due up-scaling from initial development/lab-scale to full component or structure size as well as the related up-scale from laboratory batch to full production batch size. Independent of batch size, manual FRP processing is known to yield larger scatter in FRP properties than partly or fully automated processes, see, e.g., [24]. In particular, manual cutting of the beam specimens from the manufactured test plates may yield variations in specimen width. This effect is further discussed later as well. If all FRP test specimens for a given round robin are produced from plates manufactured and cut in one single laboratory by the same technician, a fairly consistent repeatability can be achieved. “Consistent” does not necessarily imply reduced scatter in absolute terms, but limited variation among specimens. Test machine and test-rig set-up, selection of the load and displacement transducers, their measurement range or resolution and the associated sampling rates for data acquisition, the calibration of the transducers, and the proper alignment of the load introduction all contribute to extrinsic scatter. Finally, data analysis, at least as implemented in most current test standards, is also affected by choices

taken by the operators and may also yield extrinsic scatter. Of course, if manual processes are used for the manufacture of FRP components or structures, the respective scatter in the material properties must be preserved in the test specimens. Skilled process technicians, on one hand, at least to some extent, or process automation, on the other hand, will reduce the amount of scatter and provide more consistent material quality and properties. Experience at the authors laboratory has indicated that Young's modulus measurements may provide a rough quality rating for FRP: Good quality laminates yield standard deviations from testing (at least) five specimens close to 1% for CFRP and close to 3% for GFRP [25]. Higher values of standard deviation likely indicate somewhat inhomogeneous material properties, or variation in specimen size, or higher concentrations of defects. This empirical criterion may provide an order of magnitude estimate for quantification or comparison of FRP laminates with different intrinsic, material related scatter.

Mainly for multidirectional laminates, the applied loads in fracture testing (in Mode I, Mode II, Mode III, or different Mode Mixes) may lead to delamination branching or to deviation of the delamination from the plane of symmetry [26,27]. Sometimes, this is observed in cross-ply FRP laminates as well, see, e.g., [28,29]. Multiple delaminations may interact and yield significant scatter effects [30].

Recently, new processing and manufacturing routes for FRP composites are explored and developed for industrial use. These are "3D printing" or, more general, "AM" and are reviewed by, e.g., [31,32]. Both, short and continuous fiber composites can be manufactured with AM, see, e.g., [33,34], and matrix materials can be thermoplastics, see, e.g., [35,36] or thermosets, see, e.g., [37–39]. 3D printing or AM processes may yield weak interfaces and bonding between FRP layers or between fibers and matrix, prone to develop into multiple damage under service loads, or directly result in multiple defect sites and delaminations. Defects in FRP from AM are discussed by, e.g., [40–42]. The amount of defects in FRP from AM is rarely quantified, for example [43,44] report significant porosity and void contents. Service loads producing variable thermo-mechanical stresses may hence induce multiple delaminations in 3D printed or AM produced FRP composites. So far, there are no validated standard test methods available for properly quantifying and comparing propagation and potential interaction of multiple delaminations in FRP. However, delamination propagation in this case will consume more energy and that may be beneficial from an application point of view, see e.g., [45]. There are even concepts looking into implementing so-called sacrificial defects, e.g., delaminations [46] or porosity [47] for improving the overall fracture behavior.

### 3.2. Examples of "human factor" effects on fracture data and related scatter

The standard fracture mechanics tests for FRP composites typically use an artificially prepared starter crack, ideally representing what is expected to be a "natural" crack at a defined location in a specimen of defined shape and size [6]. These starter cracks then yield quantitative fracture toughness or delamination resistance values by applying standard procedures for testing and data analysis.

Some of early the fracture mechanics test standards for FRP composites were developed in the 1980ies and 1990ies when analogue data output of test machine records (e.g., on paper charts, Fig. 2 left) and manual calculation of results (Fig. 2 right) were state-of-the-art. The procedures submitted for standardization had to consider the availability of typical technology. However, the last few decades

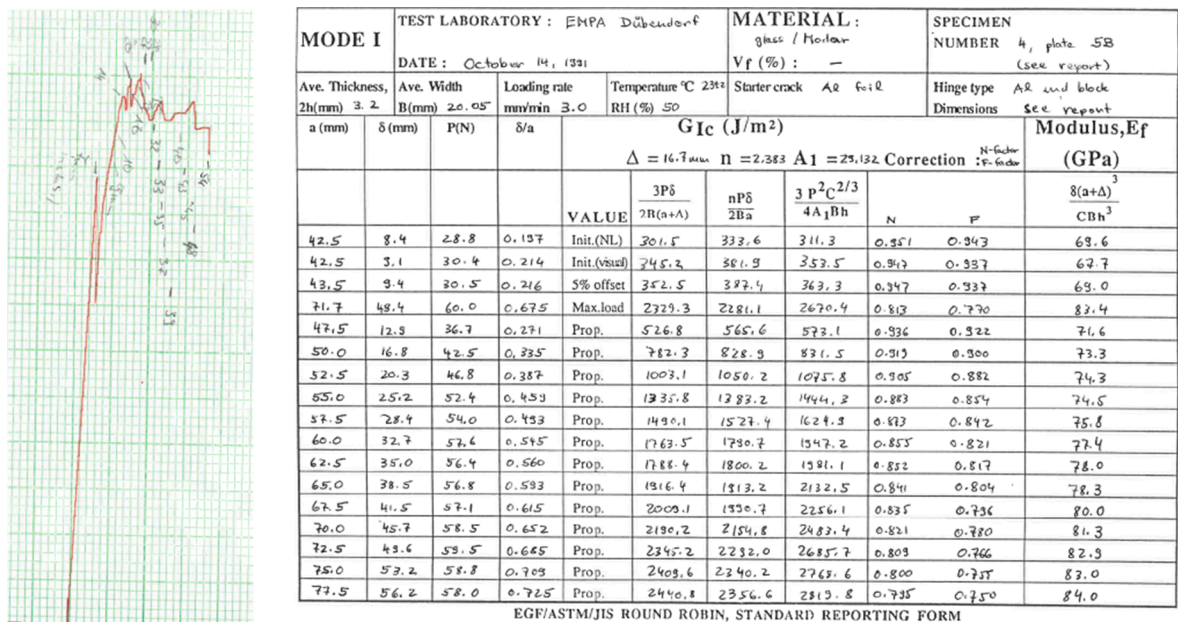


Fig. 2. (left) Analogue paper chart data record for a quasi-static fracture test, the maximum load is about 296 N, the delamination lengths from visual observation by the test operator are marked by pencil; (right) Table with data entries from manual calculations for a 1991 ESIS TC4 round robin on Mode I of GF-PMMA (selected data published in [48]).

have seen an enormous development in digital technology for measurement equipment, data recording, and computing power for analysis; also at affordable cost. This opens new opportunities for applying digital methods for testing and analysis and, possibly, reducing extrinsic scatter, as discussed in, e.g., [23]. Digital approaches that are proven to work well shall be implemented in the standard procedures, at least as options with recommendations of suitable test parameter settings.

Visual observation of the delamination propagation by the operator is, as stated above, the most obvious example of direct operator influence on the data. This is discussed in more detail in the sections below. However, as noted in [23], there are several other aspects where the human operator plays a role. “Operator” in this context does not necessarily have to be a single or the same person for all effects. As an example, the results of FRP manufacture depend on the experience of the person(s) setting-up and performing the different steps in the process. Automated processes are expected to yield consistent material quality within defined property margins better than manual manufacturing, see, e.g., [24,49]. Examples of potential scatter sources from laminate processing are fiber alignment quality, e.g., waviness, matrix porosity, internal residual stresses, but also non-uniform specimen geometry such as thickness variation. Therefore, some test standards, e.g., [50] provide limits on tolerance of width and thickness variations along the beam specimens. Test set-up and alignment of load-introduction and specimen may yield play that has to be corrected in the data analysis or possibly may produce friction affecting the load measurement. Manual definition of the cut-off points for correcting for play in the analysis of the load–displacement plots as well as the determination of the NL and 5% initiation points themselves by the operator are subjective. A round robin with more than thirty participants with experience in fracture testing has indicated significant operator dependent effects in the evaluation of NL and 5% points [51]. This round robin was using a plot of a single load–displacement trace and participants were asked to identify the NL and 5% points (not the MAX). The result indicated a 4–5% scatter in the repeatability (it was different operators judging the plot) for determining the NL delamination initiation point, and a lower scatter, but still of 2% for the 5% point when one outlier identified by Dixon’s test (a statistical test for identification of an outlier in a small sample of data [52]) was eliminated. The scatter due to operator dependent analysis of the effects of initial play in the test-rig or load-introduction has not been quantitatively assessed yet, but it may be expected to amount to a few percent as well. A digital fitting procedure recently described in [53] may provide more consistent limits for eliminating the effects of play and also for NL- and 5%-values in future data analysis. For this type of digital data analysis, the sampling rate at which the test machine records load and displacement values has to be sufficiently high, the minimum sampling rate required will depend on the loading speed. Digital analysis routines for elimination of initial play effects in load–displacement plots are expected to yield more consistent fits and data.

### 3.3. Use of simple digital tools and their effect

Likely, the first example of digital tools used in fracture testing of FRP are spreadsheets, programmed to calculate the  $G_C$ -values from load, displacement, delamination length and specimen dimensions. The first spreadsheets were introduced in the early 1990ies and made available to round robin participants [54]. An important result of using spreadsheets was that operators evaluating data manually did not always interpret the analysis procedure the way it was intended, e.g., with respect to the correction factors for load blocks and large displacements. The spreadsheets ensured a consistent way of data analysis for comparing data from different operators or laboratories. For quasi-static fracture tests, the commercial spreadsheets work well and there is a spreadsheet for Mode I

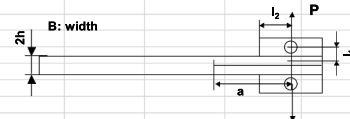
Name of the specimen: C1-9				run at 3 Hz																																																																																																																																																																																							
<div>B=20.390 mm</div> <div>2h=3.480 mm</div> <div>I1=3.850 mm</div> <div>I2=3.250 mm</div> <div>E=340000 MPa</div>				Start the calculation				<div></div>																																																																																																																																																																																			
Calibration data								Continuous data																																																																																																																																																																																			
Cycle number																																																																																																																																																																																											
new files																																																																																																																																																																																											
<table><tr><th>N</th><th>a</th><th>Pmax</th><th>δmax</th></tr><tr><th>[ ]</th><th>[mm]</th><th>[N]</th><th>[mm]</th></tr><tr><td>543</td><td>55.730</td><td>33.50</td><td>3.72</td></tr><tr><td>1028</td><td>55.850</td><td>32.53</td><td>3.72</td></tr><tr><td>3725</td><td>60.120</td><td>30.46</td><td>3.72</td></tr><tr><td>8369</td><td>60.450</td><td>30.67</td><td>3.70</td></tr><tr><td>15785</td><td>60.550</td><td>27.86</td><td>3.74</td></tr><tr><td>42807</td><td>60.900</td><td>25.99</td><td>3.72</td></tr><tr><td>71517</td><td>61.050</td><td>24.98</td><td>3.70</td></tr><tr><td>225521</td><td>65.550</td><td>23.50</td><td>3.73</td></tr><tr><td>276018</td><td>65.550</td><td>23.00</td><td>3.73</td></tr><tr><td>505813</td><td>65.680</td><td>22.16</td><td>3.70</td></tr><tr><td>577762</td><td>65.680</td><td>21.93</td><td>3.70</td></tr><tr><td>788241</td><td>65.790</td><td>21.87</td><td>3.71</td></tr><tr><td>847147</td><td>65.790</td><td>21.77</td><td>3.71</td></tr><tr><td>1526694</td><td>70.120</td><td>21.91</td><td>3.74</td></tr><tr><td>1618530</td><td>70.120</td><td>21.73</td><td>3.73</td></tr><tr><td>1782261</td><td>70.300</td><td>21.35</td><td>3.72</td></tr><tr><td>1868627</td><td>70.300</td><td>20.90</td><td>3.71</td></tr><tr><td>2044028</td><td>70.330</td><td>20.70</td><td>3.70</td></tr></table>				N	a	Pmax	δmax	[ ]	[mm]	[N]	[mm]	543	55.730	33.50	3.72	1028	55.850	32.53	3.72	3725	60.120	30.46	3.72	8369	60.450	30.67	3.70	15785	60.550	27.86	3.74	42807	60.900	25.99	3.72	71517	61.050	24.98	3.70	225521	65.550	23.50	3.73	276018	65.550	23.00	3.73	505813	65.680	22.16	3.70	577762	65.680	21.93	3.70	788241	65.790	21.87	3.71	847147	65.790	21.77	3.71	1526694	70.120	21.91	3.74	1618530	70.120	21.73	3.73	1782261	70.300	21.35	3.72	1868627	70.300	20.90	3.71	2044028	70.330	20.70	3.70	<table><tr><th>N</th><th>Pmax</th><th>δmax</th><th></th></tr><tr><th>[ ]</th><th>[N]</th><th>[mm]</th><th></th></tr><tr><td>500</td><td>34.47673</td><td>3.9937</td><td>3.7417</td></tr><tr><td>1000</td><td>33.49822</td><td>3.9510</td><td>3.6990</td></tr><tr><td>2000</td><td>32.43786</td><td>3.9520</td><td>3.7000</td></tr><tr><td>2500</td><td>31.34104</td><td>3.9530</td><td>3.7010</td></tr><tr><td>3500</td><td>31.01972</td><td>3.9528</td><td>3.7008</td></tr><tr><td>4000</td><td>30.69952</td><td>3.9515</td><td>3.6995</td></tr><tr><td>4500</td><td>30.42326</td><td>3.9510</td><td>3.6990</td></tr><tr><td>5500</td><td>30.17669</td><td>3.9533</td><td>3.7013</td></tr><tr><td>6000</td><td>30.05141</td><td>3.9546</td><td>3.7026</td></tr><tr><td>6500</td><td>29.79043</td><td>3.9546</td><td>3.7026</td></tr><tr><td>7500</td><td>29.60955</td><td>3.9500</td><td>3.6980</td></tr><tr><td>8000</td><td>29.45718</td><td>3.9510</td><td>3.6990</td></tr><tr><td>9000</td><td>29.29026</td><td>3.9507</td><td>3.6987</td></tr><tr><td>9500</td><td>29.18228</td><td>3.9509</td><td>3.6989</td></tr><tr><td>10000</td><td>29.04854</td><td>3.9522</td><td>3.7002</td></tr><tr><td>10500</td><td>28.89988</td><td>3.9524</td><td>3.7004</td></tr><tr><td>11500</td><td>28.76352</td><td>3.9504</td><td>3.6984</td></tr><tr><td>12000</td><td>28.59955</td><td>3.9497</td><td>3.6977</td></tr><tr><td>13000</td><td>28.48915</td><td>3.9508</td><td>3.6988</td></tr><tr><td>14500</td><td>28.35742</td><td>3.9534</td><td>3.7014</td></tr><tr><td>15500</td><td>28.13221</td><td>3.9501</td><td>3.6981</td></tr><tr><td>16500</td><td>28.06991</td><td>3.9545</td><td>3.7025</td></tr></table>				N	Pmax	δmax		[ ]	[N]	[mm]		500	34.47673	3.9937	3.7417	1000	33.49822	3.9510	3.6990	2000	32.43786	3.9520	3.7000	2500	31.34104	3.9530	3.7010	3500	31.01972	3.9528	3.7008	4000	30.69952	3.9515	3.6995	4500	30.42326	3.9510	3.6990	5500	30.17669	3.9533	3.7013	6000	30.05141	3.9546	3.7026	6500	29.79043	3.9546	3.7026	7500	29.60955	3.9500	3.6980	8000	29.45718	3.9510	3.6990	9000	29.29026	3.9507	3.6987	9500	29.18228	3.9509	3.6989	10000	29.04854	3.9522	3.7002	10500	28.89988	3.9524	3.7004	11500	28.76352	3.9504	3.6984	12000	28.59955	3.9497	3.6977	13000	28.48915	3.9508	3.6988	14500	28.35742	3.9534	3.7014	15500	28.13221	3.9501	3.6981	16500	28.06991	3.9545	3.7025	<div>Reduce the amount of continuous data</div> <div>Delete former results</div>			
N	a	Pmax	δmax																																																																																																																																																																																								
[ ]	[mm]	[N]	[mm]																																																																																																																																																																																								
543	55.730	33.50	3.72																																																																																																																																																																																								
1028	55.850	32.53	3.72																																																																																																																																																																																								
3725	60.120	30.46	3.72																																																																																																																																																																																								
8369	60.450	30.67	3.70																																																																																																																																																																																								
15785	60.550	27.86	3.74																																																																																																																																																																																								
42807	60.900	25.99	3.72																																																																																																																																																																																								
71517	61.050	24.98	3.70																																																																																																																																																																																								
225521	65.550	23.50	3.73																																																																																																																																																																																								
276018	65.550	23.00	3.73																																																																																																																																																																																								
505813	65.680	22.16	3.70																																																																																																																																																																																								
577762	65.680	21.93	3.70																																																																																																																																																																																								
788241	65.790	21.87	3.71																																																																																																																																																																																								
847147	65.790	21.77	3.71																																																																																																																																																																																								
1526694	70.120	21.91	3.74																																																																																																																																																																																								
1618530	70.120	21.73	3.73																																																																																																																																																																																								
1782261	70.300	21.35	3.72																																																																																																																																																																																								
1868627	70.300	20.90	3.71																																																																																																																																																																																								
2044028	70.330	20.70	3.70																																																																																																																																																																																								
N	Pmax	δmax																																																																																																																																																																																									
[ ]	[N]	[mm]																																																																																																																																																																																									
500	34.47673	3.9937	3.7417																																																																																																																																																																																								
1000	33.49822	3.9510	3.6990																																																																																																																																																																																								
2000	32.43786	3.9520	3.7000																																																																																																																																																																																								
2500	31.34104	3.9530	3.7010																																																																																																																																																																																								
3500	31.01972	3.9528	3.7008																																																																																																																																																																																								
4000	30.69952	3.9515	3.6995																																																																																																																																																																																								
4500	30.42326	3.9510	3.6990																																																																																																																																																																																								
5500	30.17669	3.9533	3.7013																																																																																																																																																																																								
6000	30.05141	3.9546	3.7026																																																																																																																																																																																								
6500	29.79043	3.9546	3.7026																																																																																																																																																																																								
7500	29.60955	3.9500	3.6980																																																																																																																																																																																								
8000	29.45718	3.9510	3.6990																																																																																																																																																																																								
9000	29.29026	3.9507	3.6987																																																																																																																																																																																								
9500	29.18228	3.9509	3.6989																																																																																																																																																																																								
10000	29.04854	3.9522	3.7002																																																																																																																																																																																								
10500	28.89988	3.9524	3.7004																																																																																																																																																																																								
11500	28.76352	3.9504	3.6984																																																																																																																																																																																								
12000	28.59955	3.9497	3.6977																																																																																																																																																																																								
13000	28.48915	3.9508	3.6988																																																																																																																																																																																								
14500	28.35742	3.9534	3.7014																																																																																																																																																																																								
15500	28.13221	3.9501	3.6981																																																																																																																																																																																								
16500	28.06991	3.9545	3.7025																																																																																																																																																																																								

Fig. 3. Example of a spreadsheet data entry template for evaluating Mode I fatigue fracture data for a ESIS TC4 round robin (provided by Dr Steffen Stelzer, Montanuniversität Leoben Austria), the partial data shown are from a round robin reported in [7].

fatigue fracture as well [7].

If fatigue fracture tests are run for several million cycles and the requirement is to record all minima and maxima of load and displacement (Fig. 3) or sufficient data points for trace fitting, the computing capacity of typical spreadsheets may not suffice. If each load cycle has to be recorded at even higher resolution, e.g., with respect to additional monitoring, such as AE [55], the analysis will require computationally more powerful software to efficiently handle the raw data.

### 3.4. How precisely can $G_{IC}$ and delamination lengths be determined?

When discussing the problem of delamination length measurement determined by visual observation and hence one of the values directly affected by the test operator, it seems worthwhile to first discuss the basic precision of the standard tests. For assessing experimental repeatability and reproducibility in round robin tests, on one hand, the measurement resolutions of the different data required or recommended in the standard test procedures, but on the other hand, also the allowed geometry tolerances have to be considered. The critical energy release rate  $G_C$  is calculated for, e.g., Mode I loading of DCB specimens as  $G_{IC}$  [16,50] from Eq. (1).

$$G_{IC} = \frac{3P\delta}{2ab} \quad (1)$$

Eq. (1) is derived from beam theory and in this form may overestimate  $G_{IC}$ . There are corrections that can be applied for root-rotation (instead of a perfectly built-in beam), load-block (stiffening a part of the beam) and large displacement effects [16,50]. However, these corrections are not considered here, since they have little effect on the comparison of scatter sources. Input values for Eq. (1) are load  $P$ , crack opening displacement  $\delta$ , specimen width  $b$ , and delamination length  $a$  (for a corresponding set of  $P$  and  $\delta$  values). Recommended specimen dimensions are length at least 125 mm, width  $b$  either 20 mm or 25 mm, and thickness  $2h$  around 3 mm for CFRP and 5 mm for GFRP [16]. In order to evaluate the effect of measurement resolution and geometry tolerance limits on  $G_{IC}$  values, an artificial data set representing a typical CF-epoxy laminate is used as example. In this set shown in Table 1, decreasing loads  $P$  are combined with increasing displacements  $\delta$  yielding the typical load-displacement curves for quasi-static Mode I tests with higher loads at low displacements and a rising R-curve with a plateau at longer delamination lengths as visualized in Fig. 4.

From Eq. (1) and the required measurement resolution and the specimen geometry tolerance limits, an order of magnitude estimate for the precision of  $G_{IC}$  is obtained. For this,  $G_{IC}$  is calculated with two data sets. The first uses values of  $P$  and  $\delta$  from Table 1 reduced by 1% and values of  $a$  increased by 0.5 mm (required measurement resolution [16]) and  $b$  increased by the tolerance limit of 0.5 mm [50] resulting in a lower bound. The second uses values of  $P$  and  $\delta$  increased by 1% and values of  $a$  reduced by 0.5 mm and  $b$  reduced by the tolerance limit (resulting in an upper bound). The comparison of these limits with  $G_{IC}$  in Table 1 yields differences of about 5.1% and 5.6% between the lower and upper bound, respectively and the average value in Table 1 (with one initiation data point yielding 7.8%). If the calculation uses a measurement resolution of 1% for the width  $b$  (i.e., 0.2 mm for 20 mm wide specimens), lower than the specified tolerance of 0.5 mm, the differences amount to between 3.7% and 4.0%, respectively (again with one initiation point yielding 6.2%).

An estimate of scatter can also be obtained using Gaussian error propagation according to Eqs. (2) and (3), see, e.g., [56] for details. This allows for identification of the relative contributions from each measured quantity due to the related measurement resolution or tolerance limit.

$$\Delta G_{IC} = \frac{d}{dP} \left| \frac{3P\delta}{2ab} \right| \Delta P + \frac{d}{d\delta} \left| \frac{3P\delta}{2ab} \right| \Delta \delta + \frac{d}{db} \left| \frac{3P\delta}{2ab} \right| \Delta b + \frac{d}{da} \left| \frac{3P\delta}{2ab} \right| \Delta a + \frac{d^2}{dP d\delta} \left| \frac{3}{2ab} \right| \Delta P \Delta \delta$$

where  $|\dots|$  indicates the absolute value, yielding, after differentiation.

$$\Delta G_{IC} = \left| \frac{3\delta}{2ab} \right| \Delta P + \left| \frac{3P}{2ab} \right| \Delta \delta + \left| \frac{3P\delta}{2ab^2} \right| \Delta b + \left| \frac{3P\delta}{2ba^2} \right| \Delta a + \left| \frac{3}{2ab} \right| \Delta P \Delta \delta$$

The cross-term with the derivatives of load and displacement is added to Eqs. (2) and (3) since these two variables cannot be considered as independent; they are correlated via the compliance or modulus of the DCB specimens. Table 2 shows the contributions to this error estimate based on Gaussian error propagation according to Eq. (3). This estimate is calculated in four ways, first taking 1%

**Table 1**

Simulated data for a quasi-static Mode I fracture test with a DCB-specimen for evaluating the effects of measurement resolution and geometry tolerance limits.

P [N]	$\delta$ [mm]	a [mm]	b [mm]	$G_{IC}$ [J/m <sup>2</sup> ]
160	1.0	51	20	235
140	1.3	52	20	263
110	1.8	53	20	280
98	2.5	57	20	322
88	3.4	60	20	374
80	4.2	63	20	400
75	4.8	66	20	409
70	5.3	70	20	398

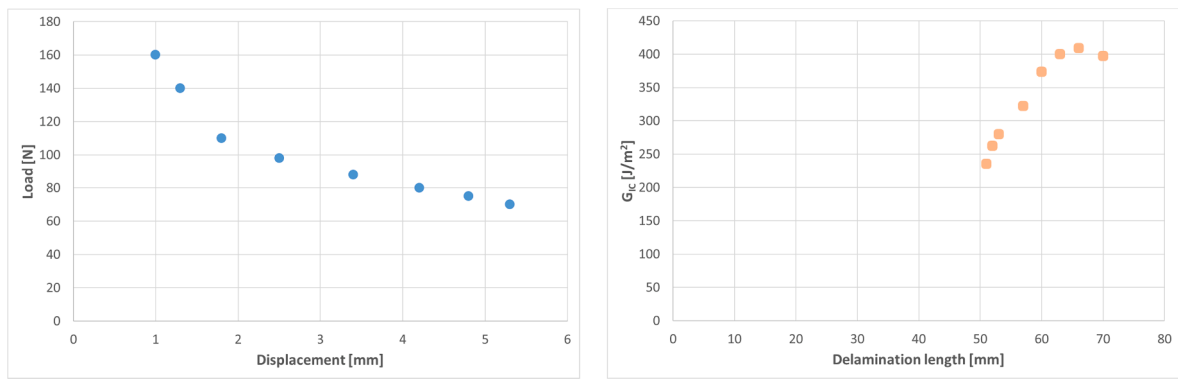


**Fig. 4.** A data set for assessing effects of measurement resolution and tolerance limits, (left) load–displacement for a quasi-static Mode I fracture test on CF-epoxy, the test starts at (0,0), (right) respective R-curve for the same data, the test starts with a starter crack length of 50 mm.

of the measured value as the resolution for each quantity including the geometric dimensions of the specimens, second and third, with two different values for tolerance limits for delamination length and, finally for the tolerance limit for specimen width. The specimen width and thickness tolerances specified in [50] amount to  $\pm 0.5$  mm and  $\pm 0.1$  mm, respectively, i.e.,  $\pm 2.5\%$  (for 20 mm width) and  $\pm 3.3\%$  (for 3 mm thickness), larger than the 1% measurement accuracy.

The resulting total error estimates between 15.9 and 23.3 J/m<sup>2</sup> for a  $G_{IC}$  of 398 J/m<sup>2</sup> (Table 1 bottom row) amount to between 4% and 5.8%. Not surprisingly, these values are similar to those from direct calculation of  $G_{IC}$  with values varying by 1% noted above. However, Table 2 further indicates that the delamination length measurement resolution of 0.5 mm will yield lower variation than the 1% for all delamination length values larger than 50 mm. Typical starter film lengths are 50 mm to 60 mm in standard Mode I DCB specimens, and the tolerance limit hence yields less than 1% scatter. If the delamination length is assumed to be determined with less precision, e.g., to 2 mm, the respective error estimate contribution is about a factor of three larger than all others (determined from 1% variation). This highlights the importance of delamination length measurement and this is further discussed in section 3.6. As detailed below, there is experimental evidence that suggests potential variations of delamination lengths between edge of the specimens and inside of several mm. Also, the total error estimate is quite sensitive to specimen geometry as shown by the last entry for specimen width variation in Table 2.

A single measurement from Eq. (3) cannot be directly compared with the round robin repeatability values stated above (resulting from an average of at least five tested specimens). However, assuming the single specimen error estimate to be representative of one standard deviation of individual specimens in an ensemble, the confidence interval of the ensemble could be estimated to amount to a value between two to three times the Gaussian error estimate for a single specimen. This rough, and, admittedly debatable, estimate, if accepted as plausible, yields values between about 10 % and 18 %. These are comparable to the experimental coefficients of variation reported as repeatability and reproducibility in round robins (Fig. 1 above). From the different contributions to the total error estimate (Table 2), it is suspected that operator performance in delamination length measurements and in specimen preparation (dimensional tolerances) are the main causes for the extrinsic scatter and these issues are now discussed in more detail.

### 3.5. Digital technology for delamination length measurements

There are several analogue or digital imaging technologies that have been applied to the determination of the delamination lengths in fracture tests instead of the subjective visual observation. In-situ X-ray projection radiography with contrast agent [57] and projection Moiré [58] are examples dating back to the 1990ies. These, however, use technology that was and probably still is not easily available in material test laboratories. Recently, several publications reported the use of digital cameras for recording either still images at selected time intervals or a full video of the specimen edge during testing, see, e.g., [59,60]. These images are evaluated manually by visual inspection or using image processing software. Digital cameras with high-resolution imaging at low cost are available, e.g., in smartphones. This would make recording of both specimen edges technically and economically feasible, in order to check for potential asymmetry in the crack tip across the width of the specimens.

**Table 2**

Contribution of each term in Eq. (3) to the total error estimate from Gaussian error propagation (evaluated for the last propagation value from Table 1), assuming 1% accuracy for each measurement, or 0.5 mm [16,50] and 2 mm, respectively for delamination length, or 0.5 mm tolerance for width  $b$ . The values shown in bold result from tolerances that are larger than 1%.

Term with	$\Delta P$	$\Delta \delta$	$\Delta b$	$\Delta a$	$\Delta P \times \Delta \delta$	Sum
a) all $\Delta = 1\%$ [J/m <sup>2</sup> ]	3.98	3.98	3.98	3.98	0.04	15.96
b) all $\Delta = 1\%$ except tolerance $\Delta a = 0.5$ mm [J/m <sup>2</sup> ]	3.98	3.98	3.98	<b>2.84</b>	0.04	14.82
c) all $\Delta = 1\%$ except tolerance $\Delta a = 2$ mm [J/m <sup>2</sup> ]	3.98	3.98	3.98	<b>11.36</b>	0.04	23.34
d) all $\Delta = 1\%$ except tolerance $\Delta b = 0.5$ mm [J/m <sup>2</sup> ]	3.98	3.98	<b>9.94</b>	3.98	0.04	21.92

The degree of automation of imaging with a camera can be increased as shown in the example of Mode I fatigue fracture tests with DCB specimens by [61], but that requires more effort in the test set-up. In this case, the camera was on one hand synchronized with the respective light source, but also with the test machine to automatically indicate the load and displacement values for each image taken by the camera. This is expected to improve the degree of consistency between the delamination lengths, load and displacement data required for calculating fracture toughness or delamination resistance and hence reduce scatter. Most test machines now allow for external signals to be synchronized with the data acquisition and hence, this could become the method of choice in the future, once the test standards provide respective requirements on such measurements.

There is also a growing number of publications discussing DIC for monitoring and evaluating the delamination length in fracture tests, see, e.g., [62–65]. Compared with digital imaging by camera, this approach requires more effort, e.g., decorating the specimen edges with a suitable speckle pattern and calibrating the cameras. DIC data analysis also requires more computational effort, but this is not a crucial limitation anymore. DIC can also be integrated into an automated test recording and analysis system, examples of that are discussed in [66,67].

A possible revision of the standard procedures shall hence define minimum requirements for imaging, e.g., still photography, video recording, DIC, for camera and image resolution, respectively, for minimum requirements on light sources, and possibly recommend suitable specimen surface preparation and frame rates for image acquisition. Periodic visual checks are still recommended for comparison with the image analysis. Delamination lengths from image analysis can further be compared with back-calculated delamination lengths from specimen compliance, see, e.g., [8] for more details.

There are other NDT methods that yield information on delamination lengths such as AE, electrical measurements, and others, see, e.g., [25]. X-ray micro-tomography has been shown to yield detailed insight into damage in FRP [68–71]. The same holds for phase-contrast, dark field X-ray radiography [72] that yields information on defect concentrations in FRP. This is possibly faster than X-ray micro-tomography, since a single image is sufficient. However, it is unlikely that these X-ray methods can easily be implemented as standard in-situ imaging tool in test machines.

### 3.6. Discussion of issues with delamination length determination

“Live” visual observation of delamination propagation with a travelling microscope by the operator has the disadvantage that there is no data record for checking on potential errors after the test and if the operator misses a reading, the information is lost and can at best be estimated, of course with limited precision. There is further the problem of synchronizing visual delamination lengths with the load and displacement record of the test machine. Even if a marker is set in the machine record (e.g., by hitting a defined key) analogous to the mark made by hand on the paper chart record (Fig. 2 left), there could be some time delay or variation (estimated to be on the order of about one-half to one second) resulting in scatter. The digital imaging tools discussed in the section above provide data that can be stored and, in principle, analyzed several times, even by different operators for assessing reproducibility. However, visual image analysis by different operators likely results in scatter due to subjective interpretation of the recorded images, yielding scatter analogous to that from direct visual observation [73].

Mode II in-plane shear loading and Mode combinations involving significant Mode II and possibly Mode III contributions are known to make visual observation challenging [74]. This is why the ISO Mode II standard procedure for FRP recommends an effective crack length approach from compliance data [75]. This, however, is based on the implicit assumption that no significant defects or damage are present or generated in the beam specimens outside the propagating delamination that could affect the compliance measurement. If this assumption is violated, such effects would tend to yield larger delamination lengths, again with respective effects in the analysis.

Even if the required resolution for delamination length measurements on the edge of the specimens of  $\pm 0.5$  mm is achieved by visual observation or other NDT, it is questionable whether these data really represent the effective delamination lengths. Fig. 5 shows two examples of delaminations from a quasi-static Mode I test performed in-situ in an X-ray radiography system, the delaminations are highlighted by opaque contrast agent. Fig. 6 shows two examples from quasi-static Mode II testing, in these cases X-ray radiography with contrast agent was performed ex-situ. Figs. 5 and 6 of X-ray radiography with contrast agent show that the tip of the delamination

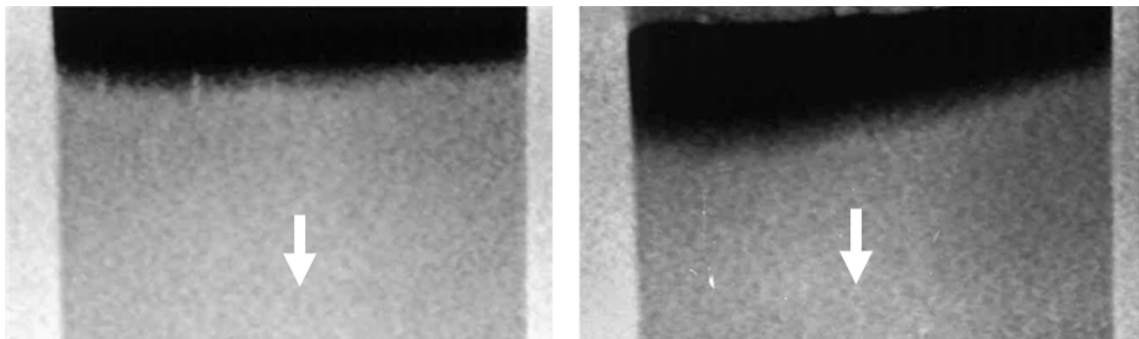


**Fig. 5.** (left) In-situ projection radiography of a Mode I CFRP DCB specimen (unpublished results from Empa), roughly symmetric delamination tip across the specimen width highlighted with a contrast agent, (right) ditto with strongly asymmetric tip, specimen widths are 20 mm for both. The white arrows indicate the direction of delamination propagation.

inside the specimens may be curved, protruding beyond the tip that is observed on the edges, or even more complex in shape with several mm between minimum and maximum positions across the specimen width. Therefore, the effective uncertainty in delamination length may be larger than the specified resolution.

For Mode I, the video recording of the delamination tip indicated by the contrast agent suggests that delamination propagation occurs by stochastic formation of small local delamination areas. These result in a somewhat corrugated form of the delamination tips across the width of the specimens. This mechanism is consistent with AE monitoring of such tests and analysis of AE recorded simultaneously with the X-ray radiography has indicated that these local delaminations have diameters on the order of a one hundred to a few hundred micrometers [76].

Of course, it is not a priori clear whether the X-ray radiography images (Figs. 5 and 6) show the “real” tip of the delamination. There are two important aspects: The first is whether the contrast agent really penetrates to the delamination tip. This requires the right combination of laminate surface wettability and contrast agent viscosity. The second is the resolution of the X-ray imaging with respect to grey-scale differences representing differences in the amount of contrast agent. A minimum amount of contrast agent is required to produce a measurable image contrast and a “sharp” tip (a few micrometers in diameter) may not contain enough contrast agent, even if penetration of the contrast agent to the tip is achieved. Hence, the tip highlighted by contrast agent may be an apparent indication rather than the effective tip as discussed, e.g., in [77]. The video recording of the delamination propagation, however, suggests that the contrast agent likely shows a self-similar shape to the tip effectively present. The use of in situ X-ray radiography for Mode I fatigue fracture tests has not been tried to the best knowledge of the author. Possibly, in situ X-ray phase contrast imaging with comparatively short image acquisition time [78,79]), may be the better approach, since it does not require contrast agent. X-ray CT imaging, on the other hand, may still require a longer duration of stopping the cyclic loading for image acquisition, e.g., a few minutes, as discussed in [71].

From the radiography images in Fig. 6 the variation in delamination length across the specimen width for Mode II loading is estimated around 1.6 mm and around 2.5 mm for GF-Polyester (Fig. 6 left) and for CF-PEEK (Fig. 6 right), respectively. For delamination lengths between 50 and 100 mm this variation amounts to between 1.5% and 3% for GF-Polyester and to 2.5% and 5% for CF-PEEK. This clearly is more than the typical 1% required measurement resolution for the other quantities (load, displacement and specimen thickness) for calculation of  $G_C$  values. The error estimate for a 2 mm delamination length variation in Table 2 confirms that delamination length may easily yield the largest contribution to the overall error value.

### 3.7. Approaches for quantification of multiple delaminations

The data analysis in the standardized test procedures as well as in the round robin guidelines for cyclic fatigue fracture implicitly assumes that one single delamination initiates from the starter crack and propagates in the mid-plane of the specimens. Delaminations deviating from the mid-plane during propagation, either fully (across the specimen width) or partially (over part of the width), often inside the specimens and hence difficult to directly observe yield detectable effects in the delamination resistance curves ( $G_{IC}$  plotted as a function of delamination length  $a$ ) as shown for the case of cross-ply laminates in [29]. DCB specimens with different thickness of the arms are discussed by [80] and DCB with asymmetric stiffness, i.e., different arms in, e.g., [81]. If delamination propagation results in crack branching, i.e., the main delamination splitting into two or more separate delaminations, even if propagating more or less in parallel, no quantitative standard analysis is yet available. Multiple delaminations may also form without branching, e.g., initiating from distributed defects in the laminates due to 3D printing and AM. This challenge is now briefly discussed.

The occurrence of multiple delaminations in different ply levels of the specimens implies some connection between the different delaminations. These connections often look much more massive (Fig. 7 left) and more complex than what is observed as so-called

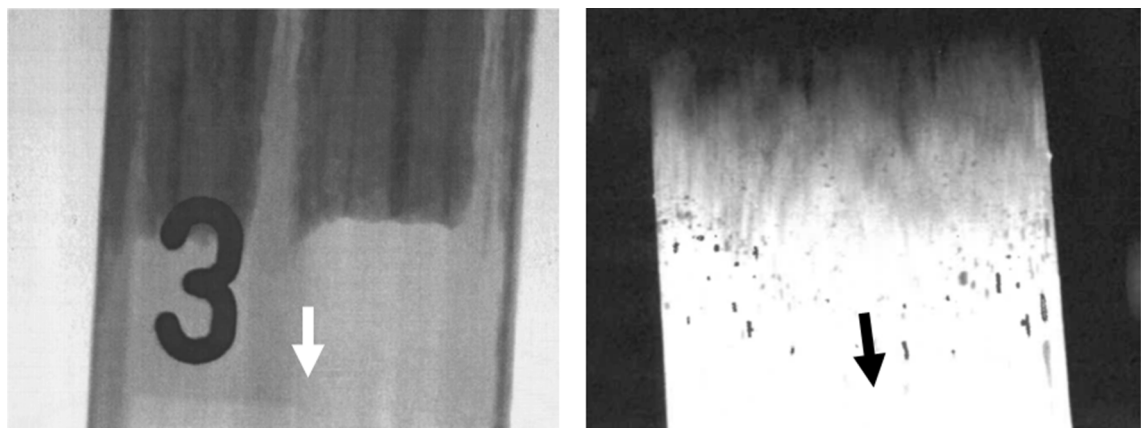


**Fig. 6.** Ex-situ radiography with contrast agent (left) of a Mode II delamination from a CDD test on GF-Polyester [77], the label “3” is a X-ray opaque marker applied for specimen identification; (right) Mode II delamination from an ENF-test on CF-PEEK, the spots below the delamination tip highlighted by the contrast agent are surface splashes from injection of the contrast agent (unpublished from Empa, courtesy of Mr. Ch. Walder), the white and black arrow indicate the direction of delamination propagation, specimen widths are 20 mm for both.

large-scale fiber-bridging in DCB specimens (Fig. 7 right), but both essentially provide some stress transfer between the two halves of the specimen beams, however, of different magnitude, until they fail.

One approach that could be applied for quantification of multiple delaminations is based on specimen compliance. Multiple delaminations in between different plies in a laminate, in principle, will have an effect on the measured stiffness. Therefore, using the crack length back-calculated from specimen compliance (essentially displacement divided by load, both measured by the test machine without operator intervention) will take any damage sufficiently affecting stiffness of the beams into account. Branched delaminations or independent multiple delaminations will thus result in a larger effective delamination length. This, however, simply interpreted as single delamination will result in lower  $G_C$  values for these specimens, in a sense underestimating their “real” delamination resistance. Multiple, sacrificial delaminations of a certain minimum size have been shown to be beneficial, e.g., by [46]. Weak layers are expected to improve delamination propagation resistance [82], since propagation of multiple delaminations yields higher energy release rates per unit length of the specimens. Possibly, the damage index developed for quasi-static Mode I tests [48] could prove useful for distinguishing between single and multiple delamination propagation in quasi-static and maybe even cyclic fatigue fracture tests. A detailed analysis of Mode I DCB tests on CF-PPS made by automated tape placement with in-situ consolidation (an AM process) with this damage parameter [83,84] looks promising, but this still requires further investigation and validation.

Another approach for quantification of multiple delaminations applies a methodology proposed to account for large-scale fiber bridging effects in cyclic Mode I fatigue fracture tests [10,11]. This fiber bridging is considered to be an artefact from the unidirectional fiber lay-up in the standard fracture specimens. Design limits for structural FRP composites that rarely have unidirectional lay-up shall hence be free of fiber bridging effects in order to be “conservative” or “safe”, if sufficient margins are defined to allow for scatter. It has to be noted that a different test yielding essentially fiber-bridging free  $G_C$  data from so-called G-constant fatigue fracture tests had been proposed a long time ago by [85,86]. In the 1990ies, the experimental set-up for such tests was rather complex and not all test machines at the time could handle the necessary type of load control. At least, the constant-G procedure will provide an independent method for validation of the approach proposed by Yao et al. [10,11].

The question whether these massive stress-transferring connections between multiple delaminations running more or less parallel to the main delamination at specimen mid-plane could be treated with the same procedure eliminating the fiber-bridging effects was also investigated in a preliminary test [83]. One single DCB specimen (again a CF-PPS made by automated tape placement with in-situ consolidation) was tested. Even though there was not a steady shifting of the fatigue fracture curves for each step of the procedure (testing delamination propagation at increasingly higher loads in each step from a new quasi-static precrack after each cyclic loading sequence) the analysis looked promising. The data points could roughly be back-extrapolated to a “bridging-free” value. Of course, this back-extrapolation is clearly affected by scatter due to the stochastic occurrence of the failure of the massive bridges that had a significant effect on the position of the fatigue fracture curves, i.e., shifting back and forth in the plot used for the analysis in some cases. Further investigations are necessary to assess the potential of this approach and to see whether it could be developed into a test standard. First, the proposed methodologies have to be validated by performing round robin tests and careful statistical analysis of the data. Nevertheless, the preliminary result looks promising and this may (once better understood and validated) provide an approach to handle multiple delaminations in FRP composites and to get some quantitative ranking with respect to delamination resistance; also for FRP made by 3D printing or AM.

#### 4. Summary and conclusions

It has been shown that intrinsic and extrinsic scatter in fracture tests on FRP composites both depend, to some extent, on decisions taken and actions performed by materials processing and test operators, respectively. Together, these significantly contribute to the empirically observed values of repeatability and reproducibility in the round robin tests, on the order of 10–20%.

The question now is: How far can intrinsic and extrinsic scatter be reduced? Likely, a promising approach to reduce intrinsic scatter is by implementing a high degree of automation, i.e., essentially digital technology, in materials processing and specimen or component manufacture with related quality control. The latter can serve as tool for identifying and, if necessary, eliminating FRP

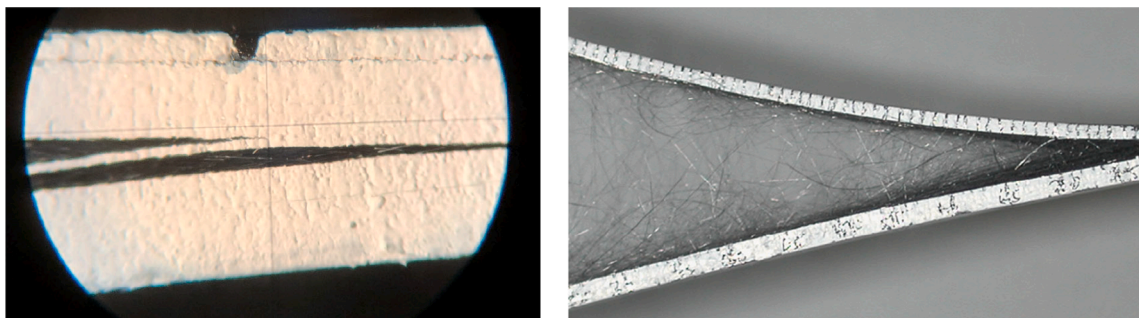


Fig. 7. Comparison between (left) delamination branching in CF-PPS DCB specimen produced with AM (courtesy Dr. M. Wolfahrt, MU Leoben), (right) large-scale fiber-bridging in CF-Epoxy DCB (courtesy Prof. B.R.K. Blackman, Imperial College); the distance between marks on the DCB specimens is 1 mm.

composite samples with properties outside specified limits. However, high degrees of automation may not always be feasible for technical or economic reasons. In particular, research and development activities may involve relatively small batches of materials not suitable for automated processing. In this case, allowing technicians to “learn”, i.e., to go through a learning curve in order to acquire the skills and experience necessary for achieving sufficiently consistent material quality [87], is a key factor. AM of FRP composite laminates, even if automated to a large extent, can still yield significant amounts of distributed defects [40–44]. In that case, development of AM technology for FRP laminates still has to reach a higher level of maturity in order to compete with existing methods. However, as indicated by the modulus measurement criterion, variation in material behavior and properties, respectively, may still yield a few percent scatter (roughly estimated to 1–3%) in repeatability or reproducibility, unless new technologies allow for higher consistency in materials processing.

The minimum extrinsic scatter, if human effects are excluded as much as possible, likely is determined by the specimen geometry tolerances set by the standards and the required measurement resolutions, the latter typically each amount to 1% of the measured value. If a lower measurement resolution would be required, this would have to be the same for all measured data, including the tolerance limits. The data simulations (Table 1 and Fig. 4) indicate a total extrinsic scatter of about 5.5%, if the tolerance in specimen width of 0.5 mm is considered. A lower tolerance value of 1% (or  $\pm 0.2$  mm) would result in reduced scatter of about 4%, but requires respective quality of machining of the specimens in order to achieve a width tolerance of  $\pm 0.2$  mm or less.

An obvious source of operator-induced scatter is the visual observation of delamination initiation and propagation (with a scatter estimated to amount up to 5%), but materials processing, e.g., affecting specimen microscopic and *meso*-scale morphology or geometry, test set-up, e.g., play in connections and friction, and manual data analysis, e.g., the determination of the NL and 5% initiation points from load-displacement records, are also sources of scatter. The latter has been shown to yield up to 5% scatter for a round robin on evaluation of a load-displacement plot, whereas for the other factors, no comparable quantitative data or estimates are available.

In order to improve precision of delamination length determination, image processing and analysis can be automated with digital algorithms for yielding more consistent values. In this context, it can be pointed out that use of digital technology does not necessarily or automatically imply higher accuracy. The discussion on the problems of delamination length determination on the edge of the specimens clearly shows that. However, more consistent data, in particular with respect to inter-laboratory comparisons, i.e., reproducibility, may already be useful with respect to definition of design limits. Depending on the type of image analysis algorithm, operator settings may still introduce some operator dependence. Recent developments in AI, e.g., integrating ML algorithms into automated image analysis systems, may provide more consistent delamination length data with less scatter [88–90].

Anyhow, it is questionable whether the indications visually or digitally detected on the edges of the specimens can be directly correlated with the effective delamination length. Additional damage occurring in the specimens during testing, outside the main delamination initiating and propagating from the starter crack as well as multiple delaminations from crack branching or distributed defects from processing, such as those induced by 3D printing or AM, so far proved difficult to quantify. Two approaches, namely determining an effective delamination length from compliance change during the test combined with a damage parameter, and a procedure recently proposed to account for large-scale fiber bridging in fatigue fracture tests seem promising for dealing with multiple delaminations. Both approaches, however, require further testing and evaluation before they can be recommended for data analysis and standardized.

Reduction of scatter from the analysis of load-displacement curves may become feasible through digital technology as well. On one hand, digital fitting procedures for effects of set-up play, NL and 5% initiation points will yield more consistent data (see, e.g., [53]) and eliminate or at least reduce the human factor. Full integration of delamination imaging for length determination with the test machine record [61] will yield more consistent raw data, i.e., triples of delamination length, load and displacement. In-situ X-ray imaging may yield more consistent information on the effective delamination area and thus improve consistency in fracture data even further, in particular in the case of multiple delaminations. However, the technology is possibly too expensive and complex for use as a standard method at this time. Future developments in miniaturization of X-ray equipment and faster imaging, however, may change this.

Overall, the discussion above indicates several aspects where digital technology can contribute to reduce scatter or at least to obtain more consistent data from given sets of raw data. In most cases, the aim is to eliminate or minimize human interference. It is estimated that with available digital technology, repeatability and reproducibility values (CV<sub>r</sub> and CV<sub>R</sub>, respectively) around 5% may be achieved. Further reduction will require improved measurement resolutions, clearly lower than 1% of all measured values and also specimen geometry tolerances of 1% or less. Nevertheless, even reducing scatter to CV<sub>r</sub> and CV<sub>R</sub> values around 5% would already constitute a significant achievement compared with the CV<sub>r</sub> and CV<sub>R</sub> values of 10–20% or more in earlier experiments.

#### *CRediT authorship contribution statement*

**Andreas J. Brunner:** Conceptualization, Formal analysis, Investigation, Methodology, Writing – original draft, Writing – review & editing.

#### **Declaration of Competing Interest**

The authors declare that they have no known competing financial interests or personal relationships that could have appeared to influence the work reported in this paper.

## Acknowledgements

Contributions of data and analysis within round robin tests from as well as many discussions with former and current members of ESIS TC4 on Fracture of Polymers, Polymer Composites and Adhesives on various aspects of fracture testing of FRP composites are gratefully acknowledged. Special thanks go to Dr Steffen Stelzer, Dr Anastasiia Khudiakova, and Dr Gaspard Clerc who in their PhD theses diligently explored several approaches, some successful, some not, to improve understanding of fracture phenomena through reduction of scatter by use of digital tools in the data analysis. Last, but not least, contributions from and discussions with many former and current staff members of the Laboratory for Mechanical Systems Engineering (the former Polymer Composites Laboratory) are gratefully acknowledged as well.

## Funding source

This research did not receive any specific grant from funding agencies in the public, commercial, or not-for-profit sectors.

## References

- [1] Jones R. Fatigue crack growth and damage tolerance. *Fatigue Fract Engng Mater Struct* 2014;37:463–83. <https://doi.org/10.1111/ffe.12155>.
- [2] Braga DFO, Tavares SMO, da Silva LFM, Moreira PMGP, de Castro PMST. Advanced design for lightweight structures: Review and prospects. *Prog Aerosp Sci* 2014;69:29–39. <https://doi.org/10.1016/j.paerosci.2014.03.003>.
- [3] Jones R, Kinloch AJ, Hu W. Cyclic-fatigue crack growth in composite and adhesively-bonded structures: The FAA slow crack growth approach to certification and the problem of similitude. *Int J Fat* 2016;88:10–8. <https://doi.org/10.1016/j.jfatigue.2016.03.008>.
- [4] Brunner AJ. Fracture mechanics of polymer composites for aerospace applications. In: Irving PE, Soutis C, editors. *Polymer Composites in the Aerospace Industry*. 2nd edition. Cambridge: Woodhead Publishing; 2020. p. 195–252. <https://doi.org/10.1016/B978-0-08-102679-3.00008-3>.
- [5] Mallick PK. Advanced materials for automotive applications: an overview. In: Rowe J, editor. *Advanced Materials in Automotive Engineering*. Cambridge: Woodhead Publishing; 2012. p. 5–27. <https://doi.org/10.1016/B978-1-84569-561-3.50014-4>.
- [6] Brunner AJ, Blackman BRK, Davies P. A status report on delamination resistance testing of polymer–matrix composites. *Eng Fract Mech* 2008;75(9):2779–94. <https://doi.org/10.1016/j.engfracmech.2007.03.012>.
- [7] Stelzer S, Brunner AJ, Argüelles A, Murphy N, Pinter G. Mode I delamination fatigue crack growth in unidirectional fibre reinforced composites: Development of a standardized test procedure. *Compos Sci Technol* 2012;72(10):1102–7. <https://doi.org/10.1016/j.compscitech.2011.11.033>.
- [8] Stelzer S, Brunner AJ, Argüelles A, Murphy N, Cano GM, Pinter G. Mode I delamination fatigue crack growth in unidirectional fibre reinforced composites: Results from ESIS TC4 round robins. *Eng Fract Mech* 2014;116:92–107. <https://doi.org/10.1016/j.engfracmech.2013.12.002>.
- [9] Jones R, Kinloch AJ, Michopoulos JG, Brunner AJ, Phan N. Delamination growth in polymer-matrix fibre composites and the use of fracture mechanics data for material characterization and life prediction. *Compos Struct* 2017;180:316–33. <https://doi.org/10.1016/j.compstruct.2017.07.097>.
- [10] Yao LJ, Alderliesten R, Zhao MY, Benedictus R. Bridging effect on mode I fatigue delamination behavior in composite laminates. *Compos Part A* 2014;63:103–9. <https://doi.org/10.1016/j.compositesa.2014.04.007>.
- [11] Yao LJ, Sun Y, Guo LC, Jia LY, Zhao MY. A validation of a modified Paris relation for fatigue delamination growth in unidirectional composite laminates. *Compos Part B* 2018;132:97–106. <https://doi.org/10.1016/j.compositesb.2017.09.007>.
- [12] ASTM D6115-97 (2019) Standard Test Method for Mode I Fatigue Delamination Growth Onset of Unidirectional Fiber-Reinforced Polymer Matrix Composites. p. 1–7. <http://doi.org/10.1520/D6115-97R19>.
- [13] Pascoe JA. Slow-growth damage tolerance for fatigue after impact in FRP composites: Why current research won't get us there. *Theor Appl Fract Mech* 2021;116 (103127):1–10. <https://doi.org/10.1016/j.tafmec.2021.103127>.
- [14] ISO 5725-1:1994. Accuracy (trueness and precision) of measurement methods and results - Part 1: General principles and definitions. p. 1–17.
- [15] ASTM D6671/D6671M (2019) Standard Test Method for Mixed Mode I-Mode II Interlaminar Fracture Toughness of Unidirectional Fiber Reinforced Polymer Matrix Composites. p. 1–15. [http://doi.org/10.1520/D6671\\_D6671M-19](http://doi.org/10.1520/D6671_D6671M-19).
- [16] ASTM D5528 (2013) Standard Test Method for Mode I Interlaminar Fracture Toughness of Unidirectional Fiber-Reinforced Polymer Matrix Composites. p. 1–13. <http://doi.org/10.1520/D5528-13>.
- [17] ISO 5725-2:2019. Accuracy (trueness and precision) of measurement methods and results — Part 2: Basic method for the determination of repeatability and reproducibility of a standard measurement method. p. 1–69.
- [18] ISO 21748:2017. Guidance for the use of repeatability, reproducibility and trueness estimates in measurement uncertainty evaluation. p. 1–38.
- [19] ASTM D7905/D7905M (2019) Standard Test Method for Determination of the Mode II Interlaminar Fracture Toughness of Unidirectional Fiber-Reinforced Polymer Matrix Composites. p. 1–18. [http://doi.org/10.1520/D7905\\_D7905M-19](http://doi.org/10.1520/D7905_D7905M-19).
- [20] O'Brien K, Martin RH. Round Robin Testing for Mode I Interlaminar Fracture Toughness of Composite Materials. *J Compos Technol Res* 1993;15(4):269–81.
- [21] Davies P, Sims GD, Blackman BRK, Brunner AJ, Kageyama K, Hojo M, et al. Comparison of test configurations for determination of mode II interlaminar fracture toughness results from international collaborative test programme. *Plast, Rubber Compos* 1999;28(9):432–7. <https://doi.org/10.1179/146580199101540600>.
- [22] Alderliesten RC, Brunner AJ, Pascoe JA. Cyclic fatigue fracture of composites: What has testing revealed about the physics of the processes so far? *Eng Fract Mech* 2018;203:186–96. <https://doi.org/10.1016/j.engfracmech.2018.06.023>.
- [23] Brunner AJ. Fracture mechanics test standards for fiber-reinforced polymer composites: Suggestions for adapting them to Industry 4.0 and the digital age. *Proc Struct Integ* 2020;28:546–54. <https://doi.org/10.1016/j.prostr.2020.10.064>.
- [24] Swan S, Yuksel T, Kim D, Gurocak H. Automation of the Vacuum Assisted Resin Transfer Molding Process for Recreational Composite Yachts. *Polym Compos* 2017;38(11):2411–24. <https://doi.org/10.1016/10.1002/pc.23826>.
- [25] Brunner AJ, Hack E, Neuenschwander J. Nondestructive Testing of Polymers and Polymer-Matrix Composites. In: Seidel A, editor. *Wiley Encyclopedia of Polymer Science & Technology*, Chichester: John Wiley & Sons; 2015. p. 1–39. <http://doi.org/10.1016/B978-0-85709-523-7.00008-6>.
- [26] Choi NS, Kinloch AJ, Williams JG. Composites under Mode I, Mode II and Mixed-Mode I/II Loading Delamination Fracture of Multidirectional Carbon-Fiber/Epoxy. *J Compos Mats* 1999;33:73–100. <https://doi.org/10.1177/002199839903300105>.
- [27] Gong Y, Zhang B, Mukhopadhyay S, Hallett SR. Experimental study on delamination migration in multidirectional laminates under mode II static and fatigue loading, with comparison to mode I. *Compos Struct* 2018;201:683–98. <https://doi.org/10.1016/j.compstruct.2018.06.081>.
- [28] Brunner AJ, Blackman BRK. Delamination fracture in cross-ply laminates: What can be learned from experiment? In: Blackman BRK, Williams JG, editors. *Proc 3rd ESIS Conference, Fracture of Polymers, Composites and Adhesives II*, ESIS Publication 32. Oxford: Elsevier; 2003. p. 433–44. [https://doi.org/10.1016/S1566-1369\(03\)80114-0](https://doi.org/10.1016/S1566-1369(03)80114-0).
- [29] Brunner AJ, Flüeler P. Prospects in fracture mechanics of “engineering” laminates. *Eng Fract Mech* 2005;72:899–908. <https://doi.org/10.1016/j.engfracmech.2004.08.002>.
- [30] Pascoe JA, Rans CD, Benedictus R. Characterizing fatigue delamination growth behaviour using specimens with multiple delaminations: The effect of unequal delamination lengths. *Eng Fract Mech* 2013;109:150–60. <https://doi.org/10.1016/j.engfracmech.2013.05.015>.
- [31] Parandoush P, Lin D. A review on additive manufacturing of polymer-fiber composites. *Compos Struct* 2017;182:36–53. <https://doi.org/10.1016/j.compstruct.2017.08.088>.

- [32] Wang YX, Zhou YH, Lin LY, Corker J, Fan M. Overview of 3D additive manufacturing (AM) and corresponding AM composites. *Compos Part A* 2020;139: 106114. <https://doi.org/10.1016/j.compositesa.2020.106114>.
- [33] Blok LG, Longana ML, Yu H, Woods BKS. An investigation into 3D printing of fibre reinforced thermoplastic composites. *Addit Manuf* 2018;22:176–86. <https://doi.org/10.1016/j.addma.2018.04.039>.
- [34] Shanmugam V, Rajendran DJJ, Babu K, Rajendran S, Veerasimman A, Marimuthu U, et al. The mechanical testing and performance analysis of polymer-fibre composites prepared through the additive manufacturing. *Polym Test* 2021;93:106925. <https://doi.org/10.1016/j.polymertesting.2020.106925>.
- [35] Caminero MA, Chacón JM, García-Moreno I, Rodríguez GP. Impact damage resistance of 3D printed continuous fibre reinforced thermoplastic composites using fused deposition modelling. *Compos Part B* 2018;148:93–103. <https://doi.org/10.1016/j.compositesb.2018.04.054>.
- [36] Luo M, Tian XY, Shang JF, Zhu WJ, Li DC, Qin YJ. Impregnation and interlayer bonding behaviours of 3D-printed continuous carbon-fiber-reinforced poly-ether-ether-ketone composites. *Compos Part A* 2019;121:130–8. <https://doi.org/10.1016/j.compositesa.2019.03.020> (am korrekten Ort oder Ming?).
- [37] Ming YK, Duan YG, Wang B, Xiao H, Zhang XH. A Novel Route to Fabricate High-Performance 3D Printed Continuous Fiber-Reinforced Thermosetting Polymer Composites. *Materials* 2019;12:1369. <https://doi.org/10.3390/ma12091369>.
- [38] Wang B, Zhang ZM, Pei ZJ, Qiu JJ, Wang SR. Current progress on the 3D printing of thermosets. *Adv Compos Hybrid Mats* 2020;3:462–72. <https://doi.org/10.1007/s42114-020-00183-z>.
- [39] Peerzada M, Ababsi S, Lau KT, Hameed N. Additive Manufacturing of Epoxy Resins: Materials, Methods, and Latest Trends. *Ind Eng Chem Res* 2020;59:6375–90. <https://doi.org/10.1021/acs.iecr.9b06870>.
- [40] Hao WF, Liu Y, Zhou H, Chen HS, Fang DM. Preparation and characterization of 3D printed continuous carbon fiber reinforced thermosetting composites. *Polym Test* 2018;65:29–34. <https://doi.org/10.1016/j.polymertesting.2017.11.004>.
- [41] Prakash RS, Karwa SS, Rajesh S, Shyam PV, Shrivastava PN. Strength and fracture behaviour of polymer matrix composite layered structures made by additive manufacturing. *Mater Today Proc* 2020;28:1030–8. <https://doi.org/10.1016/j.matpr.2019.12.347>.
- [42] Yavas D, Zhang ZY, Liu QY, Wu DZ. Interlaminar shear behavior of continuous and short carbon fiber reinforced polymer composites fabricated by additive manufacturing. *Compos Part B* 2021;204:108460. <https://doi.org/10.1016/j.compositesb.2020.108460>.
- [43] Papon EA, Haque A. Fracture toughness of additively manufactured carbon fiber reinforced composites. *Addit Manuf* 2019;26:41–52. <https://doi.org/10.1016/j.addma.2018.12.010>.
- [44] Sommacal S, Matschinski A, Drechsler K, Compston P. Characterisation of void and fiber distribution in 3D printed carbon-fiber/PEEK using X-ray computed tomography. *Compos Part A* 149;2021:106487. <http://doi.org/10.1016/j.compositesa.2021.106487>.
- [45] Peng L, Zhang JY, Zhao LB, Bao R, Yang HQ, Fei BJ. Mode I delamination growth of multidirectional composite laminates under fatigue loading. *J Compos Mats* 2011;45:1077–90. <https://doi.org/10.1177/0021998310385029>.
- [46] Herráez M, Pichler N, Botsis J. Improving delamination resistance through tailored defects. *Compos Struct* 2020;247:112422. <https://doi.org/10.1016/j.compstruct.2020.112422>.
- [47] Conway KM, Kunka C, White BC, Pataky GJ, Boyce BL. Increasing fracture toughness via architected porosity. *Mater Des* 2021;205:109696. <https://doi.org/10.1016/j.matdes.2021.109696>.
- [48] Brunner AJ, Blackman BRK, Williams JG. Calculating a damage parameter and bridging stress from GIC delamination tests on fibre composites. *Compos Sci Technol* 2006;66:785–95. <https://doi.org/10.1016/j.compscitech.2004.12.040>.
- [49] Bandekar A, Huddhar A, Desai A, Shivkumar Gouda PS. Investigations of Mechanical Behaviour of FRP Composites manufactured by the aid of Automated controlled resin Coating Process. *Mater Today Proc* 2018;5:21119–26.
- [50] ISO 15024:2001. Fibre-reinforced plastic composites — Determination of mode I interlaminar fracture toughness,  $G_{IC}$ , for unidirectionally reinforced materials. p. 1–24.
- [51] Davies P. Round Robin Analysis of  $G_{IC}$  Interlaminar Fracture Test. *Appl Comp Mats* 1996;3:135–40.
- [52] Dean RB, Dixon WJ. Simplified Statistics for Small Numbers of Observations. *Analyst Chem* 1951;23(4):636–8.
- [53] Clerc G, Brunner AJ, Josset S, Niemz P, Pichelin F, Van de Kuilen JWG. Adhesive wood joints under quasi-static and cyclic fatigue fracture Mode II loads. *Int J Fat* 2019;123:40–52. <https://doi.org/10.1016/j.ijfatigue.2019.02.008>.
- [54] Brunner AJ, Tanner S, Davies P, Wittich H. Interlaminar Fracture Testing of Unidirectional Fibre-Reinforced Composites: Results from ESIS Round Robins. In: Hogg PJ, Schulte K, Wittich H, editors. *Proc Composites Testing and Standardisation ECCM-CTS 2*. Cambridge: Woodhead Publishing; 1994. p. 523–32.
- [55] Pascoe JA, Zarouchas DS, Alderliesten RC, Benedictus R. Using acoustic emission to understand fatigue crack growth within a single load cycle. *Eng Fract Mech* 2018;194:281–300. <https://doi.org/10.1016/j.engfractmech.2018.03.012>.
- [56] Ku HH. Notes on the Use of Propagation of Error Formulas. *J Res Natl Bureau Stand - C Eng Instrument* 1966;70C(4):263–73. <https://doi.org/10.6028/jres.070C.025>.
- [57] de Kalbermatten T, Jäggi R, Flüeler P, Kausch HH, Davies P. Microfocus radiography studies during mode I interlaminar fracture tests on composites. *J Mat Sci Lett* 1992;11:543–6.
- [58] Arakawa K, Ishiguma M, Takahashi K. Study of mode I interlaminar fracture in CFRP laminates by moiré interferometry. *Int J Fract* 1994;66:205–12.
- [59] Kaushik V, Ghosh A. Experimental and numerical characterization of Mode I fracture in unidirectional CFRP laminated composite using XIGA-CZM approach. <http://doi.org/10.1016/j.engfractmech.2019.01.038>.
- [60] Ekhtiari A, Shokrieh MM, Alderliesten R. Loading rate effects on mode-I delamination in glass/epoxy and glass/CNF/epoxy laminated composites. *Eng Fract Mech* 2020;228:106908. <https://doi.org/10.1016/j.engfractmech.2020.106908>.
- [61] Chocron T, Banks-Sills L. 2019. Nearly Mode I Fracture Toughness and Fatigue Delamination Propagation in a Multidirectional Laminate Fabricated by a Wet-Layup. *Phys Mesomech* 2019;172(2):107–40. <http://doi.org/10.1134/S1029959919020036>.
- [62] Okuyama I, Koyanagi J, Arikawa S, Yoneyama S. Dynamic and static failure behavior of notched CFRP laminate investigated by digital image correlation. *Mech Time-Depend Mater* 2014;18:685–95. <https://doi.org/10.1007/s11043-013-9224-2>.
- [63] Brambleby RJ, Louca LA, Mouring SE. Influence of loading rate on the mode II fracture toughness of vinyl ester GRP. *Compos Part A* 2017;93:153–62. <https://doi.org/10.1016/j.compositesa.2016.11.023>.
- [64] Nag-Chowdhury S, Bellégu H, Pillin I, Castro M, Longrais P, Feller JF. Crossed investigation of damage in composites with embedded quantum resistive strain sensors (sQRS), acoustic emission (AE) and digital image correlation (DIC). *Compos Sci Technol* 2018;160:79–85. <https://doi.org/10.1016/j.compscitech.2018.03.023>.
- [65] Yu JT, Wang YC, Li ZH, Zhang Q, Jian XR, Zhang ZG. Using DIC technique to characterize the mode II interface fracture of layered system composed of multiple materials. *Compos Struct* 2019;230:111413. <https://doi.org/10.1016/j.compstruct.2019.111413>.
- [66] Khudiakova A, Grasser V, Blumenthal C, Wolfahrt M, Pinter G. Automated monitoring of the crack propagation in mode I testing of thermoplastic composites by means of digital image correlation. *Polym Test* 2020;82:106304. <https://doi.org/10.1016/j.polymertesting.2019.106304>.
- [67] Bak BLV, Lindgaard E. A method for automated digital image-based tracking of delamination fronts in translucent glass fibre-laminated composite materials. *Strain* 2020;56:e12345. <https://doi.org/10.1111/str.12345>.
- [68] Sket F, Rodríguez-Hortalá M, Molina-Aldareguía JM, Llorca J, Maire E, Requena G. In-situ tomographic investigation of damage development in  $\pm 45^\circ$  carbon fibre reinforced laminates. *Mat Sci Technol* 2015;31(5):587–93. <https://doi.org/10.1179/1743284714Y.00000000561>.
- [69] Wu SC, Xiao TQ, Withers PJ. The imaging of failure in structural materials by synchrotron radiation X-ray microtomography. *Eng Fract Mech* 2017;182:127–56. <https://doi.org/10.1016/j.engfractmech.2017.07.027>.
- [70] García-Rodríguez SM, Costa J, Singery V, Boada I, Mayugo JA. The effect interleaving has on thin-ply non-crimp fabric laminate impact response: X-ray tomography investigation. *Compos Part A* 2018;107:409–20. <https://doi.org/10.1016/j.compositesa.2018.01.023>.
- [71] Hanhan I, Ortiz-Morales AM, Spóano JJ, Sangid MD. Slow crack growth in laminate composites via in-situ X-ray tomography and simulations. *Int J Fat* 2022; 155:106612. <https://doi.org/10.1016/j.ijfatigue.2021.106612>.

- [72] Endrizzi M, Murat BIS, Fromme P, Olivo A. Edge-illumination X-ray dark-field imaging for visualising defects in composite structures. *Compos Struct* 2015;134: 895–9. <https://doi.org/10.1016/j.compstruct.2015.08.072>.
- [73] Amaral L, Zarouchas D, Alderliesten R, Benedictus R. Energy dissipation in mode II fatigue crack growth. *Eng Fract Mech* 2017;173:41–54. <https://doi.org/10.1016/j.engfractmech.2017.01.020>.
- [74] Blackman BRK, Williams JG. Crack length determination difficulties in composites – their effect on toughness evaluation. In: Carpinteri A, editor; *Proc 11<sup>th</sup> International Conference on Fracture ICF-11*, Torino: 2005, Paper 5722, 915–20.
- [75] ISO 15114:2014 Fibre-reinforced plastic composites - Determination of the mode II fracture resistance for unidirectionally reinforced materials using the calibrated end-loaded split (C-ELS) test and an effective crack length approach. p. 1–18.
- [76] Brunner AJ. Correlation between acoustic emission signals and delaminations in carbon fiber-reinforced polymer-matrix composites: A new look at mode I fracture test data", *Proceedings 32<sup>nd</sup> Acoustic Emission Conference (EWGAE)*, Vol. 1, Mazal P, Pazdera L editors, Czech Society for Non-destructive Testing, ISBN 978-80-214-5386-9, paper Nr. 55, p. 55–63.
- [77] Flüeler P, Brunner AJ. Investigation of Mode II Crack Propagation in Fiber-Reinforced Composite Materials Using a Setup for Curvature Driven Delamination. In: Hogg PJ, Sims GD, Matthews FL, Bunsell AR, Massiah A, editors; *Proc European Conference on Composites Testing and Standardisation ECCM-CTS 1992*, Bordeaux: European Association for Composite Materials EACM, p. 395–404.
- [78] Jerjen J, Revol V, Brunner AJ, Schuetz Ph, Kottler Ch, Kaufmann R, et al. Detection of stress whitening in plastics with the help of dark field imaging. *Polym Test* 2013;32(6):1094–8. <https://doi.org/10.1016/j.polymertesting.2013.06.008>.
- [79] Chen W, Guo Z, Hudspeth M, Parab N, Sun T, Fezzaa K. High speed X-ray PCI and XRD during Dynamic Fracture. *Proc Eng* 2017;197:278–84. <https://doi.org/10.1016/j.proeng.2017.08.105>.
- [80] Williams JG. The fracture mechanics of delamination tests. *J Strain Anal* 1989;24(4):207–14.
- [81] Ma MZ, Yao WX, Li P. Critical energy release rate for interface delamination of asymmetrical specimen. *Compos Struct* 2020;237:111919. <https://doi.org/10.1016/j.compstruct.2020.111919>.
- [82] Goutianos S, Sørensen BF. Fracture resistance enhancement of layered structures by multiple cracks. *Eng Fract Mech* 2016;151:92–108. <https://doi.org/10.1016/j.engfractmech.2015.10.036>.
- [83] Khudiakova A, Brunner AJ, Wolfahrt M, Pinter G. Quantification approaches for fatigue crack resistance of thermoplastic tape layered composites with multiple delaminations. Special Issue 'Fracture Mechanics Investigation of Polymeric Materials' Pinter G, Arbeiter F, editors, *Materials* 2021;14(6):1476. <http://doi.org/10.3390/ma14061476>.
- [84] Khudiakova A, Brunner AJ, Wolfahrt M, Wettemann Th, Godec D, Pinter G. On the investigation of quasi-static crack resistance of thermoplastic tape layered composites with multiple delaminations: Approaches for quantification. *Compos Part A* 2021;149:106484. <https://doi.org/10.1016/j.compositesa.2021.106484>.
- [85] Hojo M, Ochiai S, Aoki T, Ito H. Mode I fatigue delamination for CF/PEEK laminates using maximum-energy-release-rate constant tests (in Japanese). *J Soc Mat Sci Japan* 1995;44:953–9.
- [86] Hojo M, Aoki T. Characterization of Fatigue R-curves based on GMAX-Constant Delamination Tests in CF/PEEK Laminate. In: Thomsen O, Christian Berggreen C, Sørensen BF, editors, *Proc 20<sup>th</sup> Int Conf Compos Mat ICCM-20 2015*, Paper-ID 2116-1. p. 1–8.
- [87] Glock CH, Grosse EH, Jaber MY, Smunt TL. Applications of learning curves in production and operations management: A systematic literature review. *Comput Ind Eng* 2019;131:422–41. <https://doi.org/10.1016/j.cie.2018.10.030>.
- [88] Abu Ebayyeh AARM, Mousavi A. A Review and Analysis of Automatic Optical Inspection and Quality Monitoring Methods in Electronics Industry. *IEEE Access* 8; 2020:183192. <http://doi.org/10.1109/ACCESS.2020.3029127>.
- [89] Munawar HS, Hammad AWA, Haddad A, Soares CAP, Waller ST. Image-Based Crack Detection Methods: A Review. *Infrastructures* 6;2021:115. <http://doi.org/10.3390/infrastructures6080115>.
- [90] Klein C, Zeng QG, Arbaretz F, Devèvre E, Calderaro J, Lomenie N, et al. Artificial intelligence for solid tumour diagnosis in digital pathology. *Br J Pharmacol* 2021;178:4291–315. <https://doi.org/10.1111/bph.15633>.